**iScience, Volume *27***

## Supplemental information

# Discovery of non-genomic drivers of YAP signaling modulating the cell plasticity in CRC tumor lines

**Nobuhiko Ogasawara, Yoshihito Kano, Yosuke Yoneyama, Sakurako Kobayashi, Satoshi Watanabe, Sakura Kirino, Fausto D. Velez-Bravo, Yourae Hong, Aleksandra Ostapiuk, Pavlo Lutsik, Iichiroh Onishi, Shinichi Yamauchi, Yui Hiraguri, Go Ito, Yusuke Kinugasa, Kenichi Ohashi, Mamoru Watanabe, Ryuichi Okamoto, Sabine Tejpar, and Shiro Yui**

**Figure S1: CRC cells can be converted between proliferative 2D HC and 3D MG in vitro, Related to Figure 1**

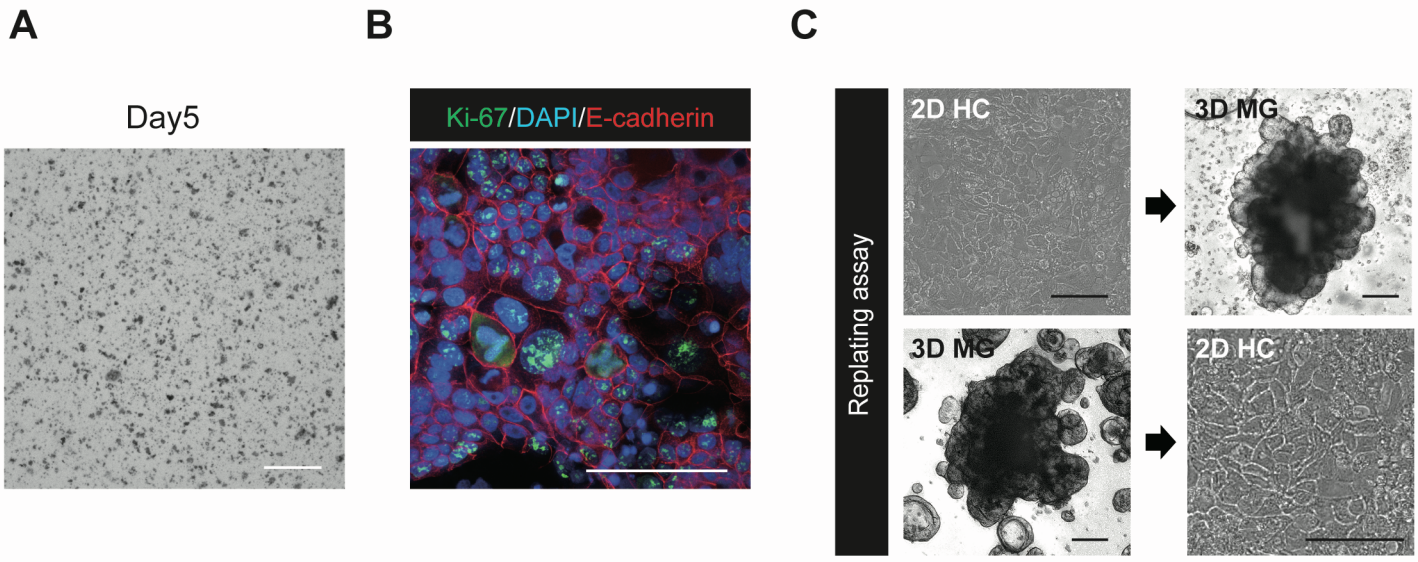

**Figure S2: The comparison between 2D HC gene set and budding signature identifies several cytoskeleton-related genes involved in tumor progression or prognosis of CRC, Related to Figure 3**

**A**

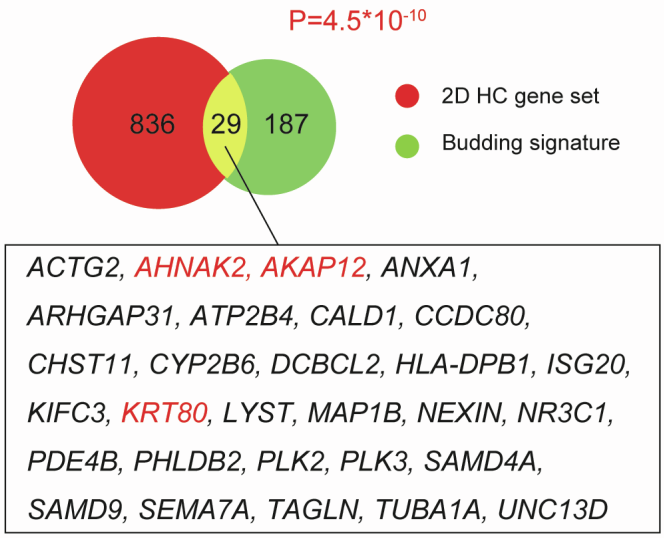


**B**

*KRT80*

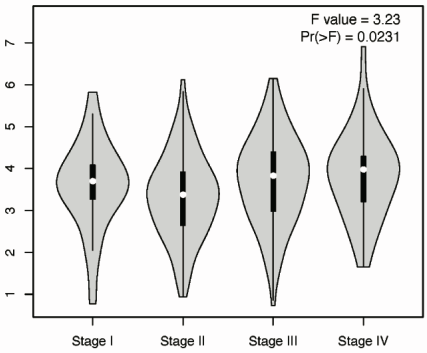


**C**

*AHNAK2*

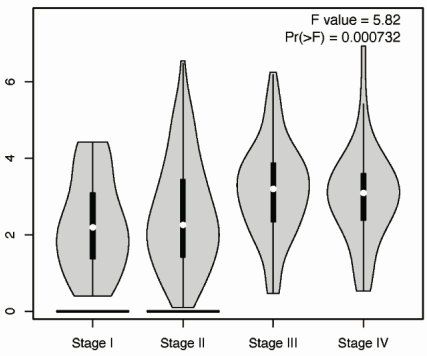


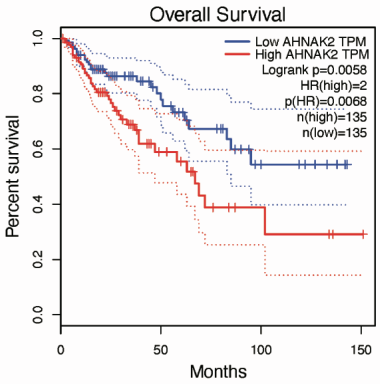


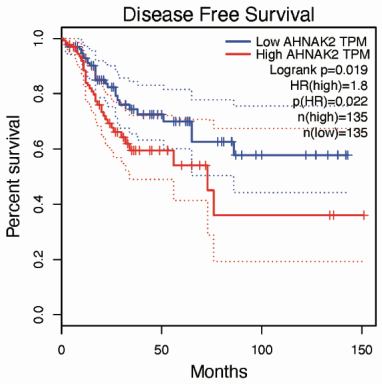


*AKAP12*

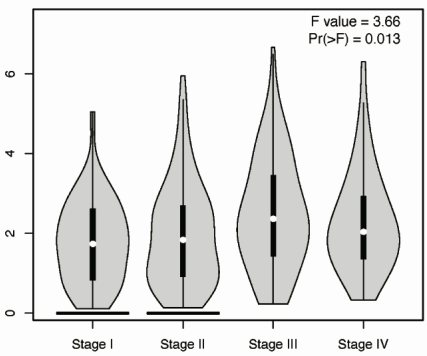


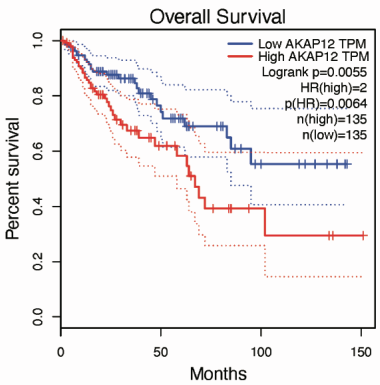


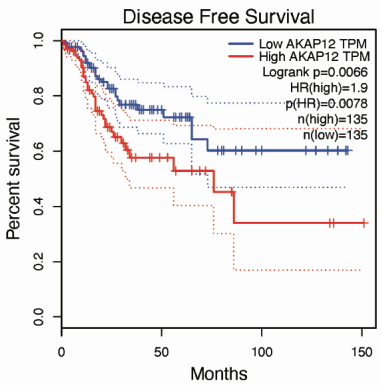

**Figure S3: Transcriptional regulatory mechanisms underlying the phenotype of 2D HC, Related to Figure 4**

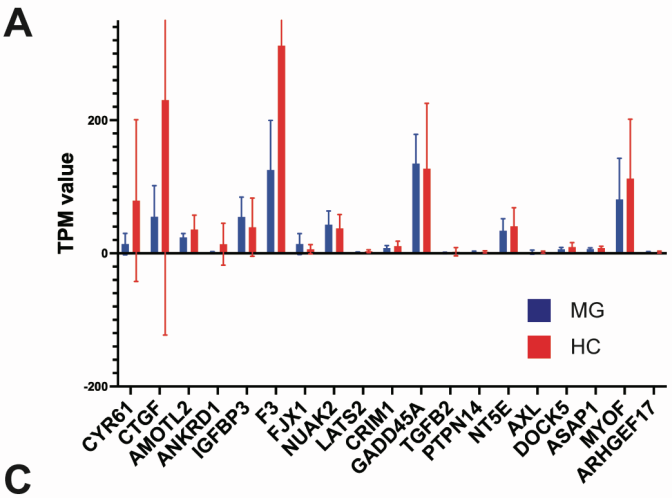


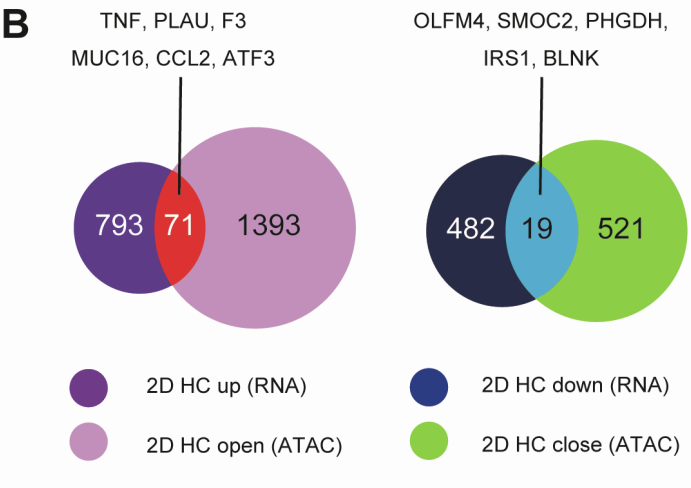


C

2D HC CLOSE

| rank | p-value | Motif | TFs |
|---|---|---|---|
| 1 | 1*E$^{-65}$ | | CDX4 |
| 2 | 1*E$^{-56}$ | | CDX2 |
| 3 | 1*E$^{-52}$ | | PPARa |
| 4 | 1*E$^{-52}$ | | HNF4A |
| 5 | 1*E$^{-51}$ | | HOXB13 |
| 6 | 1*E$^{-45}$ | | GATA1 |
| 7 | 1*E$^{-42}$ | | GATA2 |
| 8 | 1*E$^{-37}$ | | GATA6 |
| 9 | 1*E$^{-36}$ | | GATA4 |
| 10 | 1*E$^{-34}$ | | FOX |
| 11 | 1*E$^{-32}$ | | FOXA2 |
| 12 | 1*E$^{-31}$ | | RXR |
| 13 | 1*E$^{-30}$ | | P300 |
| 14 | 1*E$^{-29}$ | | HOXA11 |
| 15 | 1*E$^{-28}$ | | FRA1 |
| 16 | 1*E$^{-27}$ | | HOXD13 |
| 17 | 1*E$^{-27}$ | | FOXM1 |
| 18 | 1*E$^{-27}$ | | JUNB |
| 19 | 1*E$^{-27}$ | | FOXA3 |
| 20 | 1*E$^{-26}$ | | PPARE |
| 21 | 1*E$^{-26}$ | | BATF |
| 22 | 1*E$^{-26}$ | | FOXA1 |
| 23 | 1*E$^{-25}$ | | HOXD11 |
| 24 | 1*E$^{-25}$ | | FOSL2 |
| 25 | 1*E$^{-25}$ | | GATA3 |

2D HC OPEN

| rank | p-value | Motif | TFs |
|---|---|---|---|
| 1 | 1*E$^{-355}$ | | FRA1 |
| 2 | 1*E$^{-340}$ | | BATF |
| 3 | 1*E$^{-337}$ | | JUNB |
| 4 | 1*E$^{-335}$ | | ATF3 |
| 5 | 1*E$^{-314}$ | | FRA2 |
| 6 | 1*E$^{-308}$ | | AP-1 |
| 7 | 1*E$^{-254}$ | | FOSL2 |
| 8 | 1*E$^{-205}$ | | JUN-AP1 |
| 9 | 1*E$^{-134}$ | | BACH2 |
| 10 | 1*E$^{-44}$ | | MAFK |
| 11 | 1*E$^{-41}$ | | BACH1 |
| 12 | 1*E$^{-40}$ | | NF-E2 |
| 13 | 1*E$^{-34}$ | | NRF2 |
| 14 | 1*E$^{-29}$ | | NFE2L2 |
| 15 | 1*E$^{-26}$ | | MAFA |
| 16 | 1*E$^{-25}$ | | C-JUN |
| 17 | 1*E$^{-23}$ | | NFκB-P65 |
| 18 | 1*E$^{-21}$ | | JUND |
| 19 | 1*E$^{-20}$ | | PDX1 |
| 20 | 1*E$^{-19}$ | | TEAD3 |
| 21 | 1*E$^{-18}$ | | ATF2 |
| 22 | 1*E$^{-17}$ | | MAFB |
| 23 | 1*E$^{-17}$ | | TEAD1 |
| 24 | 1*E$^{-17}$ | | TEAD |
| 25 | 1*E$^{-16}$ | | TEAD4 |

**Figure S4: A slow-cycling 2D HC exhibiting chemoresistance to 5-FU presents higher sensitivity to TNF inhibitor, Related to Figure 6**

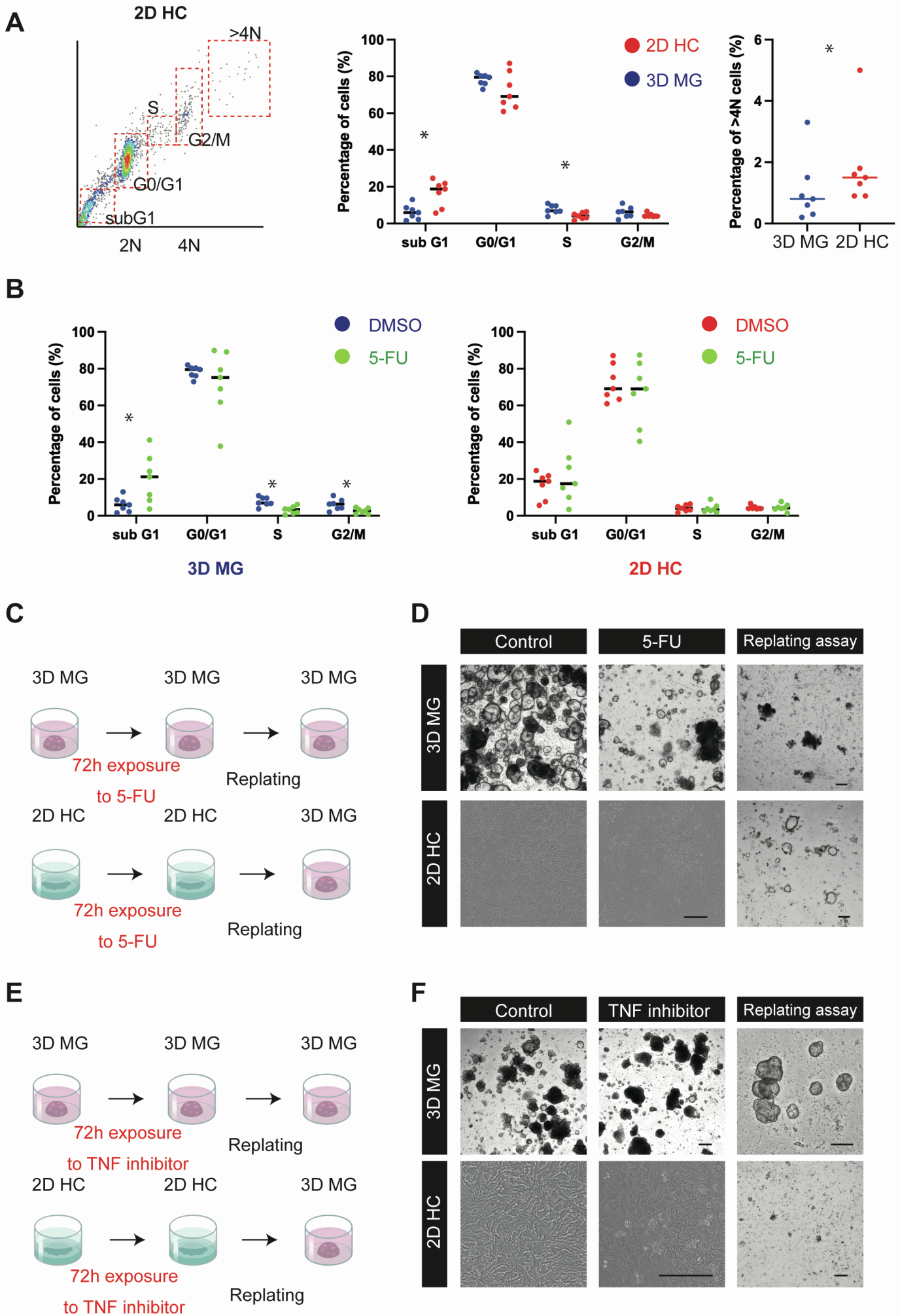

**Supplementary figure titles and legends**

**Figure S1: CRC cells can convert between proliferative 2D HC and 3D MG in vitro, Related to Figure 1**

A. The 3D method of using mixed gel composed of collagen type I, hyaluronan, and collagen type IV failed to culture CRC cells. Scale bar, 500μm.
B. An immunohistochemical image of Ki-67 (green) counterstained with DAPI (blue) and E-cadherin (red) in a monolayer culture of CRC cells (2D HC) is shown. Scale bar, 100μm.
C. 2D HC, cultured on the mixed gel composed of collagen type I, hyaluronan, and collagen type IV (HC gel), converted efficiently into Matrigel cancer organoids (3D MG) with budding structure when transferred to Matrigel (upper panel). Conversely, 3D MG could be passaged as 2D HC when seeded on HC gel (lower panel). Scale bars, 100μm.

**Figure S2: The comparison between 2D HC gene set and budding signature identifies several cytoskeleton-related genes involved in tumor progression or prognosis of CRC, Related to Figure 3**

A. A Venn diagram depicting the overlap (yellow) of 2D HC gene set (red) with budding signature (green) is shown. The p-value of statistical significance is indicated.
B. *KRT80* expression level is correlated with the histopathological stages in colorectal cancer (CRC) patients.
C. *AHNAK2* expression level is correlated with the histopathological stages in CRC patients (left panel). High *AHNAK2* expression was significantly associated with a poor overall survival (middle panel) and disease-free survival rate (right panel) in CRC patients.
D. *AKAP12* expression level is correlated with the pathological stages in CRC patients (left panel). High *AKAP12* expression was significantly associated with a poor overall survival (middle panel) and disease-free survival rate (right panel) in CRC patients.

**Figure S3: Transcriptional regulatory mechanisms underlying the phenotype of 2D HC, Related to Figure 4**

A. Total transcripts per million (TPM) values of well-established YAP target genes in 3D MG and 2D HC across all nine cases are shown. Data are represented as mean±SD.
B. The overlap (red) between 2D HC up genes (864 genes, purple) and genes showing adjacent 2D $HC^{open}$ sites (1464 sites, light red) is visualized in the left Venn diagram.

TNF, PLAU, MUC16, CCL2, and ATF3 are identified in the 71 overlapping genes. The overlap (blue) between 2D HC down genes (501 genes, dark blue) and genes showing adjacent 2D $HC^{close}$ sites (540 sites, green) is visualized in the right Venn diagram. OLFM4, SMOC2, PHGDH, IRS1, and BLNK are identified in the 19 overlapping genes.

C. The top 25 enriched transcriptional factor motifs in 2D $HC^{open}$ and 2D $HC^{close}$ sites identified in the ATAC-seq are shown.

**Figure S4: A slow-cycling 2D HC exhibiting chemoresistance to 5-FU presents higher sensitivity to TNF inhibitor, Related to Figure 6**

A. Representative cell-cycle profiling of 2D HC determined by fluorescence image cytometer NucleoCounter NC-250™ system is shown in the left panel. Each cell population in the subG1, G0/G1, S, and G2/M phases is indicated by a dashed square, respectively. The multinucleated cell population (>4N cells) is also surrounded by a dashed square. Quantification of cells in the subG1, G0/G1, S, and G2/M phases is shown in the middle panel, and that of cells with >4N DNA content is shown in the right panel. Quantification is measured in the percentage of total cells in seven cultures of 3D MG and 2D HC. Statistical significance: $*p<0.05$, paired t-test.
B. Quantification of cells in the subG1, G0/G1, S, and G2/M phases following the treatment of 5-FU at 40μM, measured in the percentage of total cells in 7 cultures of 3D MG (left panel) and 2D HC (right panel) is shown. Statistical significance: $*p<0.05$, paired t-test.
C. A schematic presentation of the replating assay following the treatment of 5-FU in both 3D MG and 2D HC is presented. In the assay, 3D MG (upper panel) or 2D HC (lower panel) is firstly exposed to 72h treatment of 5-FU at 40μM. After exposure, both materials are replated and continued to be cultured as 3D MG.
D. Representative images of 3D MG (upper panel) and 2D HC (lower panel) after 72h treatment of DMSO (control) and 5-FU at 40μM are shown in the left and middle panels, respectively. Representative microscopic images of 3D MG and 2D HC in the replating assay are shown in the right panel. 2D HC shows tolerance to 5-FU treatment. Scale bars, 200μm in 3D MG, and 100μm in 2D HC.
E. A schematic presentation of the replating assay following the treatment of a TNF inhibitor in both 3D MG and 2D HC is presented. In the assay, 3D MG or 2D HC is firstly exposed to 72h treatment of a TNF inhibitor at 10μM. After exposure, both materials are replated and continued to be cultured as 3D MG.
F. Representative images of 3D MG (upper panel) and 2D HC (lower panel) after 72h

treatment of DMSO (control) and a TNF inhibitor at 10μM are shown in the left and middle panels, respectively. Representative images of 3D MG and 2D HC in the replating assay are shown in the right panel. Scale bars, 200μm in 3D MG, and 100μm in 2D HC. 2D HC shows an apparent culture deficiency after a TNF inhibitor treatment.